Limb observations of CO2 and CO non-LTE emissions in the Venus atmosphere by VIRTIS/Venus Express

G. Gilli, Miguel Lopez-Valverde, Pierre Drossart, Giuseppe Piccioni, Stéphane Erard, Alejandro Cardesin Moinelo

Limb observations of CO_2 and CO non-LTE emissions in the Venus atmosphere by VIRTIS/Venus Express

G. Gilli,[1] M. A. López-Valverde,[1] P. Drossart,[2] G. Piccioni,[3]
S. Erard,[2] and A. Cardesín Moinelo[3]

Received 11 February 2008; revised 29 October 2008; accepted 13 November 2008; published 7 March 2009.

[1] We report and analyze here observations of strong infrared emissions from the limb of the Venus upper atmosphere during daytime, taken by the Visible and Infrared Thermal Imaging Spectrometer (VIRTIS) aboard Venus Express. We focus on the measurements taken during the first 4 months of nominal operations. The emissions observed at 4.3 μm and at 2.7 μm are attributed to CO_2 fluorescence of solar radiation and are detected up to about 160 km and 130 km, respectively, while the CO fluorescence at 4.7 μm is observed up to about 120 km. The emissions are detected in both the channels of VIRTIS, at different spatial and spectral resolutions (resolving powers about 1800 and 400), for the periapsis and the apoapsis of the Venus Express orbit. From these data sets we built up 2-D maps of the emissions as well as vertical profiles, which are then studied in order to characterize their variations with geophysical parameters, like solar illumination and emission altitude. Several analyses are performed in order to understand the VIRTIS behavior, to determine systematic effects in the data, and to propose appropriate corrections. We also present comparisons with a theoretical nonlocal thermodynamic equilibrium (non-LTE) model of the Venus upper atmosphere. The agreement is very encouraging, in general, and the main variability observed in the data, with solar zenith angle and altitude, can be understood with the model. We conclude that the present data set opens brilliant perspectives for deriving densities and rotational temperatures in the upper mesosphere and lower thermosphere of Venus.

Citation: Gilli, G., M. A. López-Valverde, P. Drossart, G. Piccioni, S. Erard, and A. Cardesín Moinelo (2009), Limb observations of CO_2 and CO non-LTE emissions in the Venus atmosphere by VIRTIS/Venus Express, *J. Geophys. Res.*, *114*, E00B29, doi:10.1029/2008JE003112.

1. Introduction

[2] The European mission Venus Express arrived at Venus in April 2006, and started its scientific phase in June 2006, being the first mission in more than 20 years to study the Venus atmosphere systematically from orbit [*Svedhem et al.*, 2007]. In contrast to the Earth's mesosphere and lower thermosphere, the equivalent density layers on Venus from about 90 to 150 km, are regions scarcely observed using remote sounding in the infrared (IR). The most abundant species CO_2, is well known to present strong IR vibrational-rotational bands, and more than 25 years ago, Pioneer Venus made systematic nadir observations using the fundamental band of CO_2 at 15 μm in order to retrieve atmospheric temperatures in the mesosphere of Venus [*Taylor et al.*, 1980]. Also, NIMS/Galileo permitted a sounding of the lower mesosphere temperature at 4.3 μm in nadir and nighttime [*Roos-Serote et al.*, 1995]. However, at higher altitudes, these emissions are expected to be out of thermodynamic equilibrium, with particularly large deviations during daytime, owing to solar pumping of the corresponding vibrational states [*Dickinson*, 1972; *Deming et al.*, 1983; *Roldán et al.*, 2000]. As a consequence, their inversion in terms of geophysical parameters is not straightforward, or in other words, their thermodynamic information content is limited [*López-Puertas and Taylor*, 2001]. The understanding of these non-LTE emissions is important, not only for its own interest, but also they can give rise to a large radiative heating, or cooling, of the atmosphere. In the case of Venus, they are a key ingredient of the energy balance between 80 and 150 km [*Bougher et al.*, 1994]. *Roldán et al.* [2000] showed that the CO_2 bands at 4.3 μm and the ones at 2.7 μm dominate the solar heating at those altitudes; much less important are the CO absorptions at 4.7 μm, given the lower atmospheric abundance of CO. Further observational problems challenged an infrared sounding of these layers from the Venus orbit so far; among them, the pointing in the limb (the optimum geometry of observation at these low atmospheric densities) and the sensitivity of the infrared detectors.

[3] Progress toward limb sounding of planetary atmospheres has been made during the last 2 decades, both theoretically and observationally. Triggered by ground-based

[1]Instituto de Astrofísica de Andalucía, CSIC, Granada, Spain.
[2]Observatoire de Paris, Meudon, France.
[3]IASF, INAF, Rome, Italy.

0148-0227/09/2008JE003112

observations of CO_2 laser bands at 10 μm, a number of non-LTE models for atmospheric IR emissions were developed for Mars and Venus in the 1980s [*Deming et al.*, 1983; *Gordiets and Panchenko*, 1983; *Stepanova and Shved*, 1985]. Later, more comprehensive tools were developed in preparation for sounding of the Martian atmosphere in the IR during the 1990s [*López-Valverde and López-Puertas*, 1994], which were adapted later to the Venus atmosphere [*Roldán et al.*, 2000]. These models, which included many more radiative bands and CO_2 energy states, represent adequate tools for simulation and analysis of limb data. Some of the few non-LTE observations available so far, and amenable for such studies, were taken by the Near Infrared Mapping Spectrometer (NIMS) instrument [*Carlson et al.*, 1992] on board the Galileo sounder, during its flyby of Venus in 1990 [*Carlson et al.*, 1991]. A few limb spectra of the CO_2 4.3-μm band were obtained during daytime and were explained recently using an improved version of the non-LTE model of Roldán and colleagues [*López-Valverde et al.*, 2007] (hereinafter LVEA). Recent analysis of CO_2 non-LTE emissions have also been carried out for Mars using data from the Planetary Fourier Spectrometer (PFS) on board Mars Express [see *López-Valverde et al.*, 2005; *Formisano et al.*, 2006], which helped to partially validate the non-LTE model. Regarding CO, non-LTE emission lines in the near-IR were first discovered in the Venus atmosphere about 20 years ago by *de Bergh et al.* [1988]. They were recently modeled and analyzed by *Crovisier et al.* [2006], who identified the fundamental CO(1-0) and the first hot CO(2-1) vibrational-rotational bands, derived rotational temperatures from them, and predicted that the instrument VIRTIS/Venus Express might detect these emissions.

[4] VIRTIS is one of the instruments aboard Venus Express with capabilities to sound the upper atmosphere of Venus [*European Space Agency* (ESA), 2001; *Titov et al.*, 2006]. It is an imaging spectrometer in the visible and near infrared, inherited partly from the Rosetta mission [*Coradini et al.*, 1998]. VIRTIS is devoted to a large number of investigations at Venus, like the cloud deck morphology and dynamics, the lower atmospheric composition, and the derivation of the temperature structure in the lower mesosphere. First studies of these aspects are presented in companion papers in this issue. Most of these studies are carried out by nadir observations. However, VIRTIS is designed to perform limb observations aboard Venus Express as well [*Titov et al.*, 2006]. This mode of observation represents the first systematic sounding of the upper layers of the Venus atmosphere in the infrared, and is devoted to understand the Venus high-atmosphere emissions [*Drossart et al.*, 2007b]. The detection of the non-LTE CO_2 4.3-μm band by VIRTIS at thermospheric altitudes has been confirmed by *Drossart et al.* [2007a], in consonance with the theoretical expectations.

[5] In this paper, we focus on a detailed and systematic analysis of VIRTIS observations of CO_2 and CO non-LTE emissions from the upper atmosphere of Venus using such a limb geometry. This is a unique data set, and our goals include, first of all, performing an internal validation of the data of our interest, second, characterizing the behavior of the instrument during limb sounding, and also describing the data set available, its quality and quantity, and its scientific potential. These CO_2 non-LTE emissions have also been observed by VIRTIS in nadir, which show signatures of gravity waves propagation into the thermosphere, as studied in a companion work in this issue [*García et al.*, 2009]. The study of the O_2 infrared system in the Venus mesosphere is also presented by *Hueso et al.* [2008] and in this issue (G. Piccioni et al., Near IR oxygen nightglow observed by VIRTIS in the Venus upper atmosphere, submitted to *Journal of Geophysical Research*, 2009).

[6] In this paper we also present and discuss comparisons with the non-LTE model results in LVEA, using both their published results and a small number of specific simulations performed here with such model. Although a more detailed comparison between model and data is under preparation, this is the first time that this model is confronted with an extensive data set of such a high spectral and spatial resolution. This work is, therefore, also devoted to test the model's main theoretical predictions, and to identify improvements and lines of exploration for non-LTE models.

[7] In section 2, we first describe VIRTIS observations in the limb, including the presentation of 2-D maps and vertical profiles of radiances. Their validation analysis, including consistency tests, actual noise level determination, as well as internal correlations and comparisons with the non-LTE model, are presented in section 3. Further discussions, future prospects and conclusions, are presented in section 4.

2. VIRTIS Observations

[8] VIRTIS on Venus Express is an imaging spectrometer whose precursor is currently en route to comet 67P/Churyumov-Gerasimenko, as part of the scientific payload of the Rosetta mission. Its detailed description and calibration can be found elsewhere [*Coradini et al.*, 1998; *Piccioni et al.*, 2006; *Titov et al.*, 2006] and see also the companion papers in this issue. We briefly describe here those characteristics and mode of operation on board Venus Express which are needed for our analysis.

2.1. VIRTIS/VEX Characteristics and Data Set

[9] The instrument consists of two channels: VIRTIS-M (hereinafter V-M), a mapping spectrometer at a resolving power $R \sim 400$, working in the visible (0.3–1 μm) and in the near infrared (1–5 μm), and VIRTIS-H (hereinafter V-H), a high-resolution spectrometer ($R \sim 1800$) working in the spectral range 2–5 μm. Table 1 of the work by *Drossart et al.* [2007b], summarizes their main characteristics; let us recall some of them here. The nominal field of view (FOV) is 64 $\times$ 64 mrad^2 for V-M (whole frame, with 256 spatial pixels in each direction), and 0.58 $\times$ 1.75 mrad^2 for V-H. The V-M spectral range is sampled at 432 spectral wavelengths, while a typical V-H spectrum obtained in the nominal mode contains a sequence of 3456 measurements. The nominal noise equivalent radiance (NESR), for 1 second of integration time, is 5000 μW m^{-2} sr^{-1} μm^{-1} in both channels, according to the *ESA* [2001]. All V-H and V-M data taken during one orbit, or terrestrial day, are stored in the so-called "qubes." The V-M ones generally contain a set of data in 3 dimensions, 2 spatial and 1 spectral. During each orbit the number of V-H/V-M data qubes

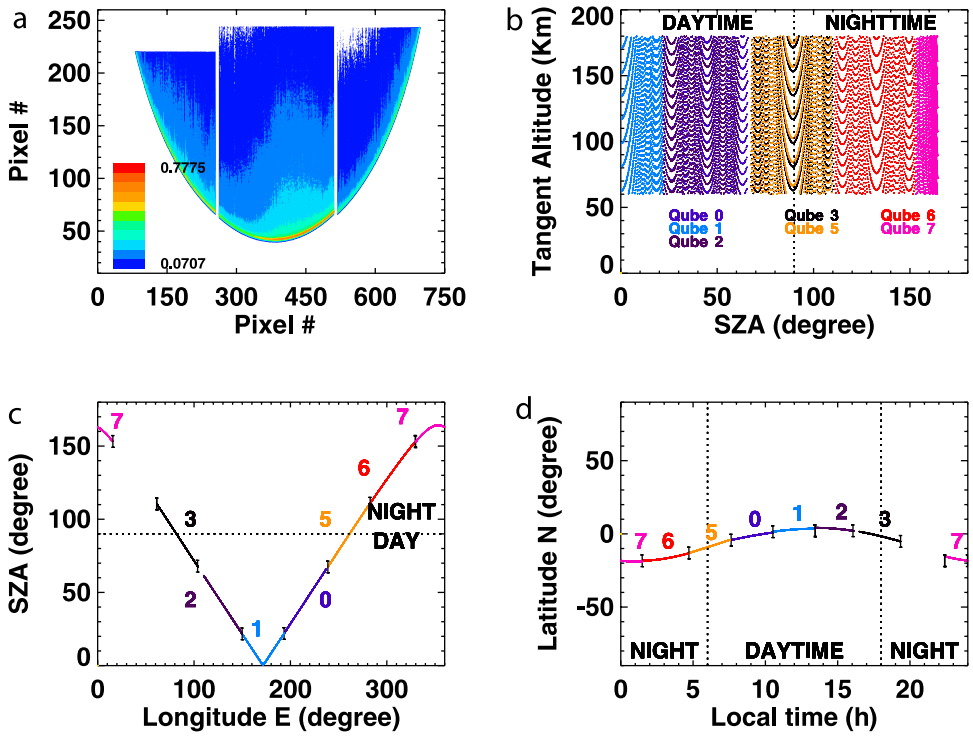

Figure 1. Geographical coverage with VIRTIS-M (V-M) during orbit 25, from apoapsis. (top, left) Map of radiances at 4.32 μm from qubes 0, 1, and 2. (top, right) Altitude-SZA location of all the limb data above the cloud layer (all pixels of seven qubes of this orbit); (bottom) Location of the data in SZA, longitude, latitude, and local time. The numbers identify the different qubes.

obtained varies from 1 to 20. A detailed description of data handling and archiving is presented by *Drossart et al.* [2007b].

[10] VIRTIS observations are separated into two categories, corresponding to distances of Venus Express to the planet lower than 12,000 km (Spectral Mode) or higher (Spectral Imaging Mode). During the Spectral Mode only a partial coverage of the surface is normally obtained, but thanks to the proximity to the planet, a very small field of view (projected) is achieved, ideal to study atmospheric variability and composition, and for tangential limb observations. Several instruments on board Venus Express share this operation mode. The Spectral Imaging Mode permits unique and unprecedented maps of the disk of Venus, and has been used to obtain global observations from apoapsis ("mosaic construction"). We will show below how these VIRTIS 2-D images contain useful information on the limb of the planet as well.

[11] A note regarding the distinction between limb and nadir observations is needed in order to clarify that, in a general sense, a data qube from VIRTIS will contain both kind of observations. Our distinction merely tells whether the line of sight touches the disk of Venus (nadir data) or crosses its atmospheric limb. Therefore, some pixels may represent actual limb sounding while nearby pixels in the same V-M image will supply "disk" observations. This will become clearer in section 2.5. For this reason, analysis of nadir observations, described in companion papers of this issue, share similar difficulties to our study and all of them are beneficial to the overall validation of VIRTIS data.

2.2. Geographical and Temporal Coverage

[12] At present, V-M data are available in calibrated form up to the orbit 631 (13 May 2006 to 1 Jan 2008), but in this work we focused our analysis on a selected number of orbits up to orbit 295 (10 February 2007). For V-H, at the time of preparing this paper, the data from orbit 23 to 127 (13 May 2006 to 25 August 2006) were already calibrated, so we focused on them, while only a fraction was calibrated and available for the rest of the mission. As mentioned above, our purpose is to perform an exploration of V-M and V-H limb data in the Venus upper atmosphere, from the cloud top, around 60 km, up to upper thermospheric layers. With this aim, we made a catalog of orbits/qubes/pixels with actual limb sounding and a number of diagrams of the geometrical and spatial coverage of all limb data obtained. Examples are shown and commented next.

2.2.1. VIRTIS-M

[13] Starting with V-M, Figures 1 and 2 show two examples of the V-M coverage for two different observational geometries, both sampling the Venus limb, one from orbit 25 (15 May 2006), during the apoapsis, and the other from orbit 43 (2 June 2006) near the periapsis. They can be considered as representative of the two principal VIRTIS modes of observation (see section 2.1).

[14] The first orbit, from apoapsis, contains 8 qubes of V-M data (7 with limb data), each one consisting of set of pixels, or a 2-D image at each wavelength, as mentioned above. Let us recall that each pixel is associated to one individual spectrum. In Figure 1a, data at the wavelength of 4.32 μm from three of the qubes, building up a map of radiances; we will discuss them below. Each qube includes a

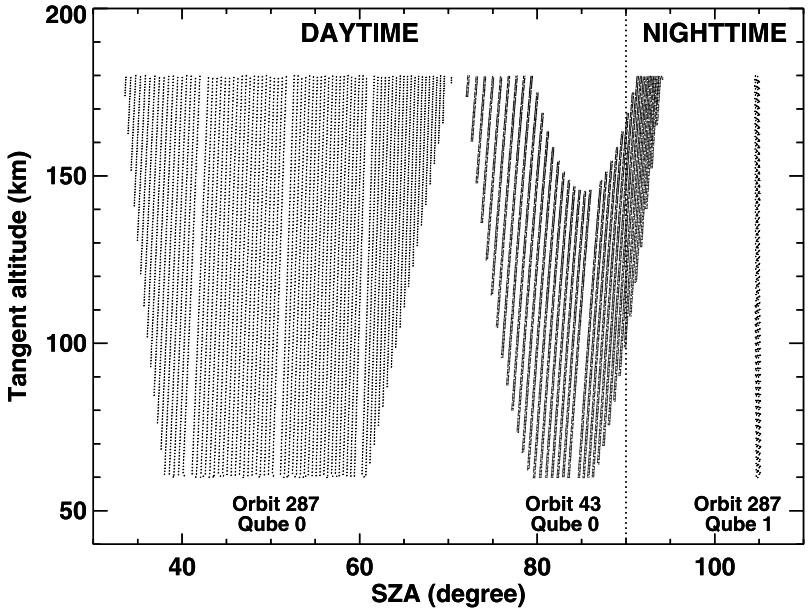

Figure 2. V-M coverage in tangent altitude versus SZA during periapsis of orbits 43 and 287. Data are shown between 60 and 180 km only.

large number of pixels (245 × 256), and the fraction of those pixels with actual pointing to the Venus limb are shown in Figures 1b–1d. We see that when the 8 qubes are considered, the latitude, longitude, and local time of the data cover an ample range of values. In this work we pay particular attention to the altitude and solar zenith angle (SZA) coverage. These two parameters are expected to produce the maximum variation in the non-LTE emission of both CO_2 and CO in the atmosphere, according to the model of LVEA. The most intense signal is expected between 90 and 140 km, and for low SZA values; for nighttime the signal would be very low, and we confirmed all of this with VIRTIS data. Figure 1b shows that the number of limb daytime spectra is large for this orbit. The vertical resolution from each row of pixels (for each qube) is between 15 and 20 km, typically. This is larger than an atmospheric scale height, but the superposition of adjacent rows may improve significantly this resolution, as we will show below. Also the SZA sampling is not completely even, but the large density of points permits suitable averaging if they are needed.

[15] Figure 2 illustrates the V-M coverage in the qube 0 of orbit 43 (2 June 2006), during the periapsis of Venus Express and in the qubes 0 and 1 of the orbit 287 (1 February 2007). We use again altitudes at the tangent point versus SZA, which describe our preferred data set for limb sounding. The available daytime limb data during the orbit 43 are about 5410 while this number is larger for the 287 (about 8000). The vertical resolution obtained at the limb from one single row of pixels (∼300 m), improves by a very large factor with respect to the apoapsis case, and is therefore particularly useful for studying the vertical variation of the non-LTE emissions and testing the theoretical predictions.

2.2.2. VIRTIS-H

[16] Observations of the limb of the planet by VIRTIS in the Spectral Mode are not as frequent as in the Spectral Imaging Mode owing to pointing constraints; the field of view of the V-M frame is much larger than the V-H. The amount of V-H spectra which actually touches the limb of the planet is therefore very limited in most orbits, sometimes only 2 or 3 spectra of our interest are available per orbit.

[17] Figure 3 illustrates the V-H geometrical coverage at the limb, again as a function of SZA and tangent altitude, combining all the orbits during the first four months of operation. A total of 651 points are shown, each one representing a V-H spectrum. We have marked 4 specific orbits (43, 76, 80, and 88) to indicate 4 different special observational coverages. The first one corresponds to a special limb case, the so-called "Tangential Limb Scenario" [see *Titov et al.*, 2006], where the satellite is fixed pointing to the limb of Venus during the periapsis. This is a specially useful kind of orbit for limb sounding and for non-LTE studies, given the high rate of tangent point observations. Orbit 76 (6 July 2006) corresponds to a "stellar occultation" case, where again a large number of observations is obtained at the limb, but they correspond to the nighttime hemisphere. They do not show a distinct emission level and have not been considered in the analysis. The other two orbits correspond to the most common limb scenario.

[18] For a number of studies, averaging of these data may be required, in order to achieve a good SZA or altitude coverage. From the 651 V-H limb spectra available, a total of 145 are daytime observations (SZA < 90°), and 44 of these correspond to strong solar illumination conditions (SZA < 60°). The last ones are, in principle, optimum for non-LTE studies. Let us recall that, within Venus Express, V-H data are the measurements with the highest spectral resolution. The latitude and longitude coverage of the daytime spectra are shown in Figure 3 as well. Except for orbits 43 (2 June 2006) and 80 (10 July 2006), with high-latitude sampling of nearby points, all others are disperse, with a preference for low latitude.

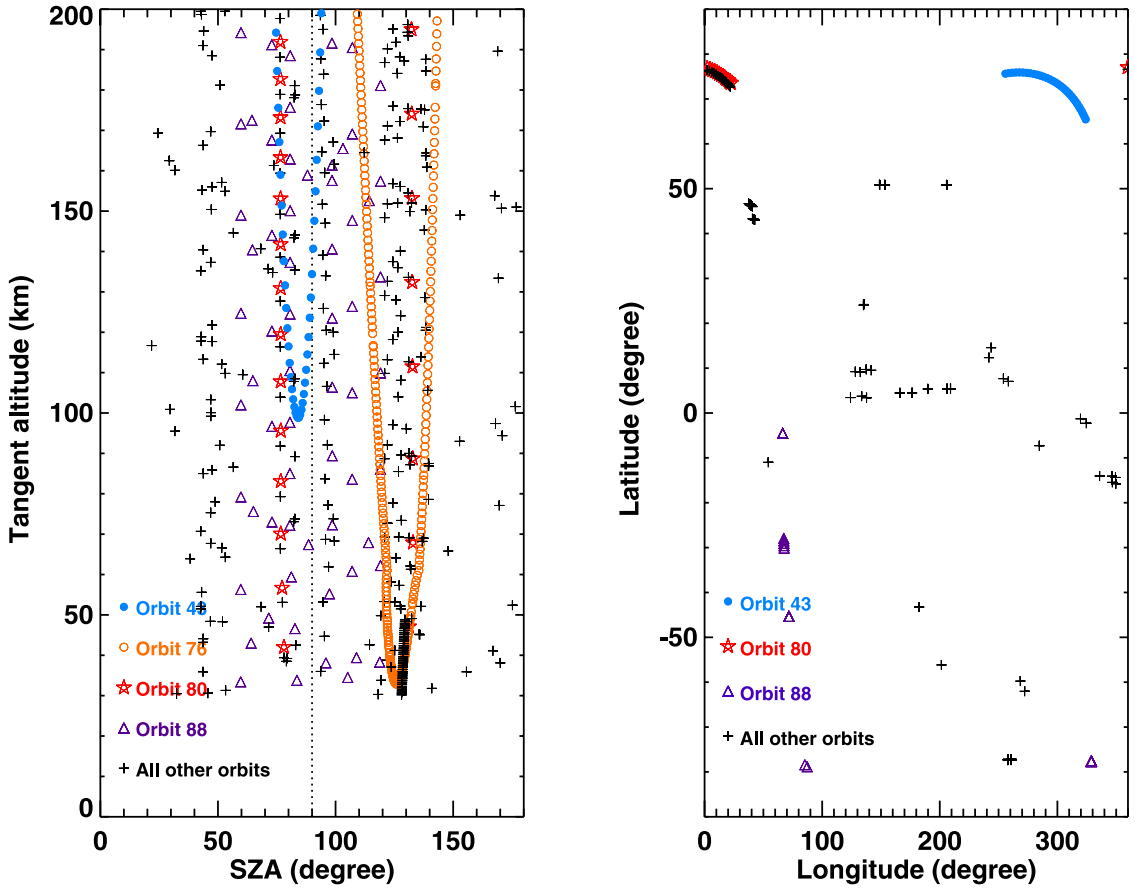

Figure 3. (left) Coverage in tangent altitude and SZA of the VIRTIS (V-H) data available from all the orbits from 23 to 127. Some orbits are indicated with special symbols. (right) Latitude-longitude location of the data, for daytime only. Symbols as in the left. See section 2.2.2 for details.

2.3. VIRTIS-H Spectra and Profiles

[19] We describe here typical V-H limb spectra which show strong non-LTE signals, and we build up vertical profiles also, in order to characterize the emissions. We focus on three emission bands, those at 4.3 μm and 2.7 μm both due to CO_2, and that at 4.7 μm, due to CO. All of them are suitable to be contrasted with the recent non-LTE model predictions of LVEA.

2.3.1. CO_2 4.3 μm Emission

[20] Figure 4 (left) shows a sample of seven V-H spectra in the 4.3-μm region, corresponding to different orbits, and pointing at different tangent altitudes. The selection corresponds to orbits 33, 40, and 47 (24 May, 31 May, and 7 June 2006, respectively) and to a SZA interval from 20° to 30°. First, it is noticeable an intensity of the signal well above the noise level at all wavelengths between 4.20 and 4.50 μm. The emission falls to zero shortward and longward of these values, respectively, where the small oscillation observed can be considered as the measurement noise and which seems to be close to 2000 μW m^{-2} sr^{-1} μm^{-1}. Only the two lowest altitude spectra show signal in the wings, though surely from solar scattering in the clouds. At the uppermost altitude shown in Figure 4, 167 km, the spectrum is still above noise level, which demonstrate that V-H can sound up to those thermospheric altitudes in Venus before averaging.

[21] It is clear that the spectral shape of the 4.3-μm band, the peak intensity, and the wavelength of the peak of the band, vary with altitude. The maximum emission is obtained in this sample around 110 km tangent altitude. This is close to the altitude predicted by the CO_2 non-LTE model by LVEA. Also the spectral shape is similar to the model prediction, with three clear peaks in the 110 km spectrum, around 4.28, 4.32 and 4.35 μm. According to the model, the first peak is due to the second hot band of the main CO_2 isotope; the mechanism being solar absorption at 2.7 μm, exciting CO_2 states which later relax radiatively, emitting in the 4.3-μm region. The second peak, around 4.32 μm, is produced by radiative relaxation of the CO_2 vibrational states excited after solar absorption at 2.7 μm and 2.0 μm. The third peak is mostly due to solar pumping at 2.0 μm. The non-LTE model predicts that at high tangent altitudes the 4.3-μm band would change this shape to a simpler two emission peaks separated by a dent around 4.29 μm, due to the dominance of the 2.7 μm solar pumping. This is indeed observed in Figure 4, above about 130 km. At higher altitudes, the model predicts a further change, due to the direct solar absorption in the fundamental band of the main isotope, whose central dip at 4.26 μm is observed in Figure 4 in the 167 km spectrum.

[22] Vertical profiles can be constructed combining spectra at different altitudes. They, however, will not represent

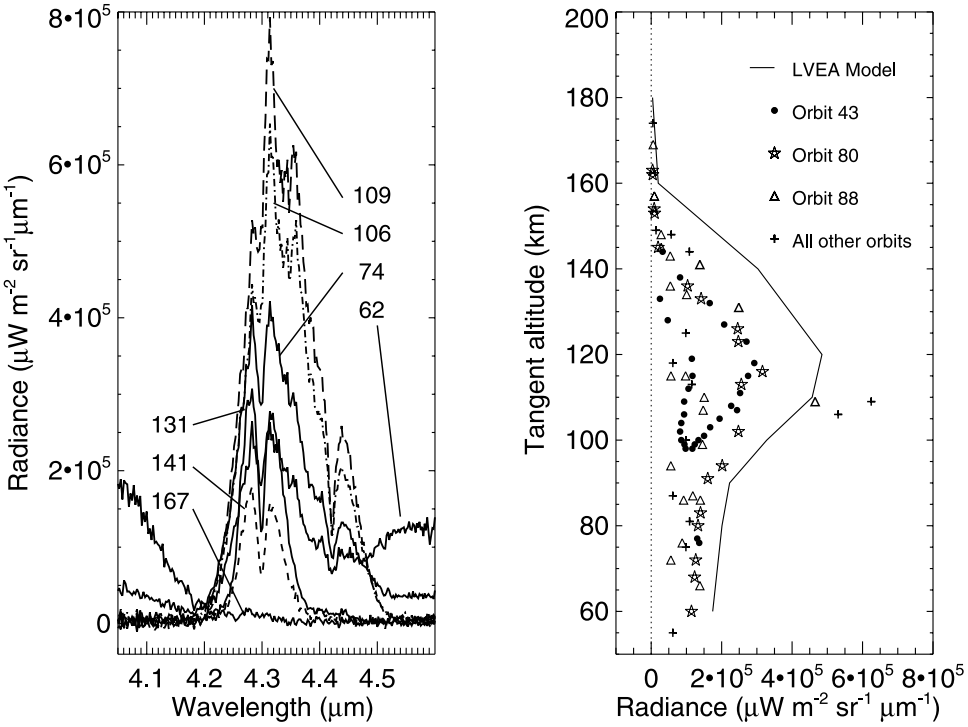

Figure 4. (left) Selection of seven V-H spectra from orbits 33, 40, and 47 at different altitudes and for $20° < SZA < 30°$. (right) Vertical distribution of the 145 daytime measurements at 4.32 μm from orbits 23 to 127 (May–August 2006). The solid line on the right represents a model simulation. Orbits and symbols as in Figure 3.

real 1-D profiles of the Venus atmosphere. Only a couple of orbits (43 and 80) contain a sufficient number of limb spectra to build a vertical profile for one single orbit; in general, data from different dates and geographical locations will be combined. This will have to be taken into account when performing detailed comparisons with non-LTE models, which usually provide the radiance structure at a single geographical location. In Figure 4 (right) we combine diverse data at 4.32 μm. The data and the symbols correspond to those in Figure 3. A tentative grouping by SZA values did not show any clear trend, given the scarcity of data; the SZA variation is better observed in V-M data and discussed below.

[23] The cloud of V-H data presents a dispersion not present in the 1-D radiance simulations by LVEA, also shown in Figure 4. The model simulation corresponds to SZA = 80° similar to that of orbit 80. This orbit can be considered as a good 1-D profile extending from 30 to 200 km. Notice that data from orbit 43 can also be used to build vertical profiles, but only above about 100 km. Both data and model present a clear increase with altitude in the lower mesosphere and a peak emission around 120 km. Above this altitude, the emission declines quickly to zero, following the decrease in atmospheric density. The actual atmospheric density profile is critical in determining the precise altitude of the peak emission, and this is the most likely reason for the mismatch with the prediction of LVEA. Regarding the peak radiances, not much comparison can be performed at this stage, as it should be the topic of a more rigorous comparison of the non-LTE model, and should account for suitable atmospheric variability in the density profiles.

2.3.2. CO_2 2.7 μm Emission

[24] According to LVEA, CO_2 emissions at 4.3 μm and at 2.7 μm are both produced by solar pumping. The emission level at 2.7 μm is, however, much lower and we have only found a small number of cases/spectra with a distinct emission above noise levels. Figure 5 shows two of those spectra, which correspond to SZA of about 45° and 60°. One of them presents a bias, which is not corrected here. A non-LTE model simulation has been performed for these solar illumination conditions, using the VIRA reference atmosphere, and is also presented in Figure 5. The spectral shape of the two fundamental bands of the main CO_2 isotope can be discerned, by comparing with the non-LTE model simulation. The data are very noisy for further conclusions at this stage. Hopefully, a more extended data set of V-H spectra will be obtained during the rest of the mission, and a statistically sounded comparison with the theoretical prediction will be a good test for non-LTE models. This 2.7 μm non-LTE emission has also been detected in the V-M signal, as we discuss in section 3.2.

2.3.3. CO 4.7 μm Emission

[25] Figures 6 and 7 illustrate a similar study for the 4.7-μm spectral region which, according to LVEA is dominated by non-LTE emissions of CO in the upper mesosphere and lower thermosphere. The emission observed is lower than the CO_2 emission, and the number of V-H CO spectra with good signal to noise ratio is much smaller. About 20 spectra, out of the 145 available at the limb during daytime, show a clear signal. Many of them show a small signal above the noise level or above the daylight scattered by the aerosols and clouds. This is why it is difficult to detect this non-LTE

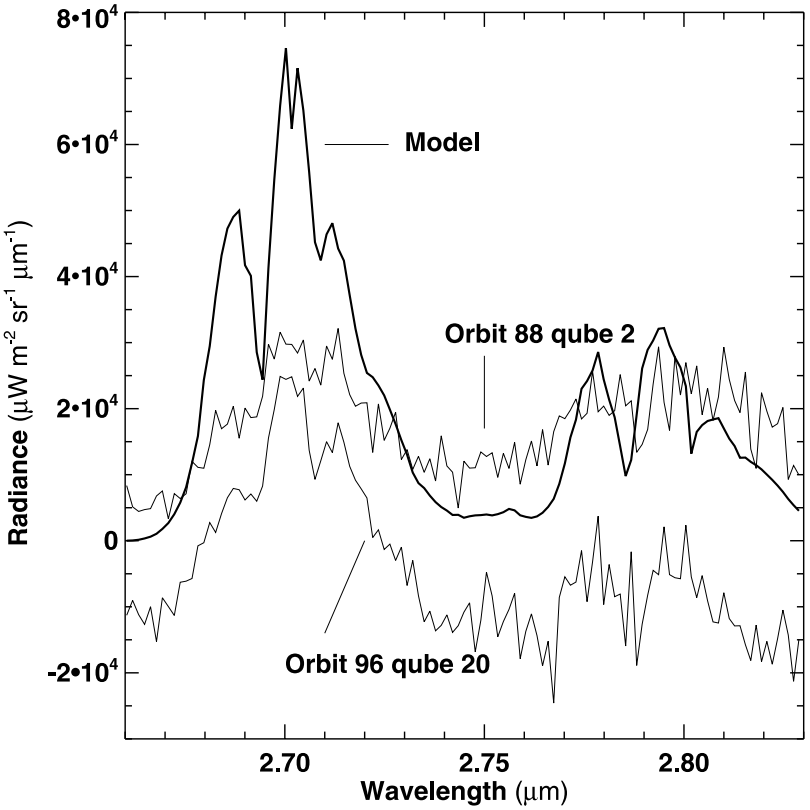

Figure 5. Two selected spectra at 2.7 μm observed by VIRTIS-H (thin lines) compared to a non-LTE model simulation (thick line). The upper spectrum is from orbit 88, qube 2 at an altitude of about 107 km and SZA about 60°. The lower spectrum is from orbit 96, qube 20 at an altitude of 118 km and SZA about 45°. The theoretical simulation has been performed at 110 km and for similar solar illumination conditions. No shift has been applied to the observed data. See section 2.3.2.

emission below about 70 km. The highest altitude where the emission can be clearly identified is about 120 km.

[26] Three of the most interesting spectra are shown in Figure 6 (top). The two spectra with the strongest emission correspond to two observations at approximately the same tangent height, around 85 km, but for SZA of 60° and 76°. The third one, shifted downward for clarity, is the spectrum at the highest altitude available in the data set explored so far, about 120 km. In spite of the noise level, very noticeable in the high-altitude spectrum, and which amounts to $\sim$5000 μW m^{-2} sr^{-1} μm^{-1}, in all of them we can see two branches of what seems a typical vibrational-rotational band. The simulations of LVEA for the CO(1-0), or fundamental band (FB), of the main isotope showed such structure as well. However, their prediction has a minimum emission at the FB center, at 4.67 μm, while the spectra in Figure 6 present their central minimum around 4.73 μm. This points to a different band of CO, the CO(2-1), or first hot (FH), of the main isotope, as responsible for these data. Such emission was not simulated by LVEA, who focused their analysis in the FB. These V-H measurements indicate that, if the fundamental transition is present, its intensity is smaller than the first hot. A similar effect was observed with ground-based measurements at much higher spectra resolution [see *Crovisier et al.*, 2006].

[27] The spectral resolution of V-H allows to identify individual lines of the P and R branches of the FH CO band, and this is shown Figure 6 (bottom). A number of vertical lines are drawn at the wavelengths of the spectral lines centers of the two bands, according to HITRAN [*Rothman et al.*, 2005]. For clarity, we focus on the spectral interval occupied by the P branch of the FH band. We can identify most of the lines of the P branch, up to P20 at least. It is interesting to notice, however, that in the center of the FH P branch, at 4.727 μm, a weak emission line is observed, which coincides with the line P7 of the CO fundamental band. No FH lines are present there. Moreover, all the 5 lines observed around this wavelength are better fit by the P5–P9 lines of the FB than by the FH band. In other words, the emission from the FB seems to be also detected in the central portion of the FH band. The absence of FH lines may be due to the smaller strength of the lines with low rotational number. This is a tentative explanation which requires careful quantitative modeling.

[28] As previously done by *Crovisier et al.* [2006], it might be possible to derive temperatures from this emission after a correct model fit. This is not possible with the model of LVEA in this moment, but we have attempted to estimate the rotational temperature from some VIRTIS data. First, we assumed that the rotational levels of CO are in thermal equilibrium at the pressures of relevance. Then, the usual expression for the rotational temperature, given by the ratio of line intensities (see an example for the Venus atmosphere by *Deming et al.* [1983]), was applied to the spectrum shown in Figure 6 (bottom). A selection of lines from the P branch of the FH band is required. The criteria we

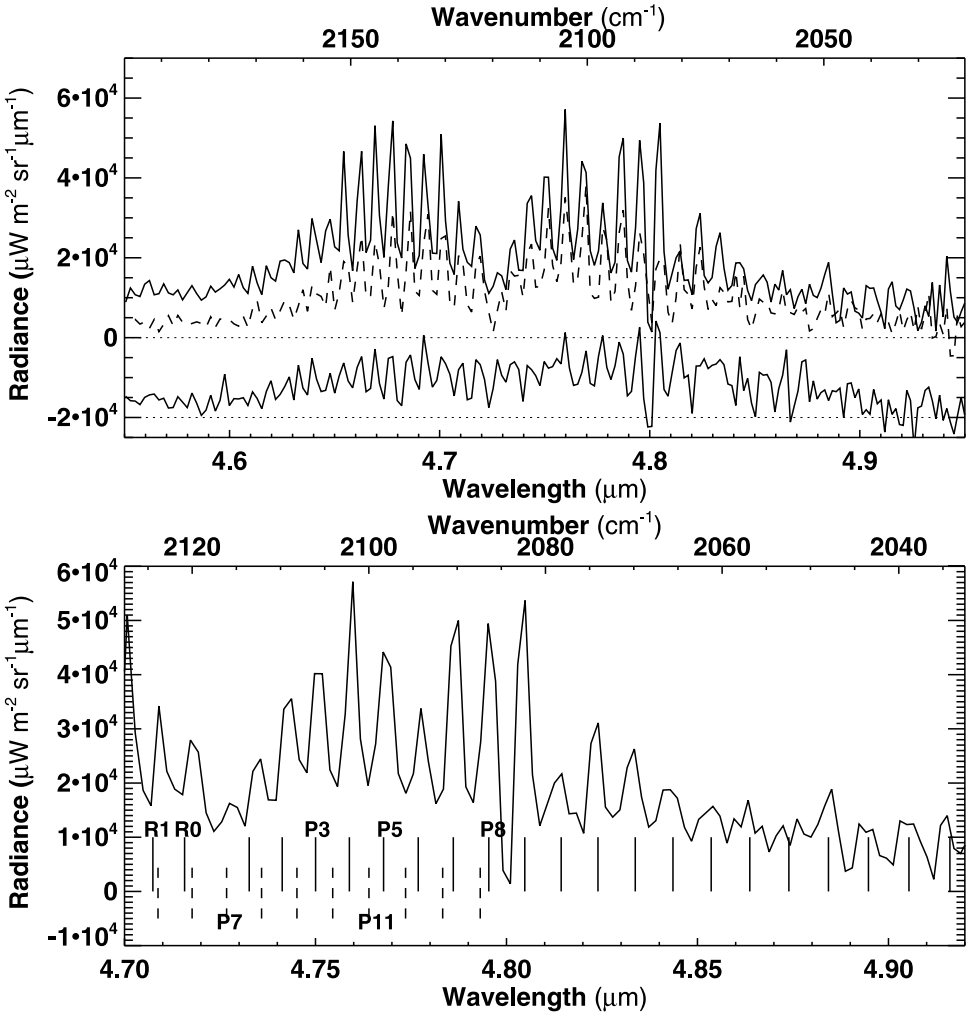

Figure 6. (top) Selection of three V-H spectra at 4.7 μm. The two closer ones correspond to about 85 km and to SZA of 60° (solid line) and 76° (dashed line). The lowest spectrum, shifted 20,000 radiance units downward for clarity, corresponds to a tangent altitude of 118 km and SZA of 46°. (bottom) Zoom of the SZA 60° spectrum, with lines marking the positions of the Hitran line centers for the fundamental (dashed marks) and first hot (solid marks) bands of CO.

followed were a small overlapping with the FB lines and a peak emission well above the noise levels. This method rules out high and low J lines. Also, adjacent rotational lines should be avoided in order to reduce numerical error. For this spectrum, the best subset of lines that we found are those between P3 and P8. By forming pairs between the more extreme ones, P3, P4 and P7, P8, several values of rotational temperature were found, all around 237 K, but with uncertainties of 50 K or larger. This large error is due to the large sensitivity to the peak intensity in the center of the lines. This intensity value is uncertain because it is not directly available from the data, given the V-H spectral resolution and sampling, but obtained by an extrapolation to the radiance values in the centers of the selected lines. Notice that the P branch of this spectrum apparently has a maximum at P9 and a local minimum at P6; we have excluded these two lines in this analysis since they seem specially affected by the V-H sampling and noise. This error in the lines intensities can be reduced in the future, by using a non-LTE model simulation for the FH band, as was done by *Crovisier et al.* [2006].

[29] Regarding the vertical variation, profiles can be constructed from the two dozens of spectra with good S/N ratio. They are shown in Figure 7 at 4.678 μm. The data have a clear dispersion, and in contrast to the model prediction for the FB, it does not show any clear peak: the plateau between 95 and 120 km, at about 6000 μW m^{-2} sr^{-1} μm^{-1} is very close to the noise level. As it happened with the CO_2 data in Figure 4, the small number of points does not allow to discern a clear SZA variation.

2.4. VIRTIS-M Maps During Periapsis

[30] In this section we present measurements of V-M from the periapsis, where the maximum spatial resolution can be achieved, as shown in Figure 2. In the Spectral Mode, near periapsis, the V-M slit is fixed, no scanning is performed, and a row of pixels is taken. Therefore, the mapping is composed of a set of successive "V-M slit frames," each one taken about 10 s apart, while the spacecraft is moving along the orbit.

[31] This is illustrated in Figure 8, where we plotted a map of CO_2 radiances at 4.32 μm, in the center of the strong

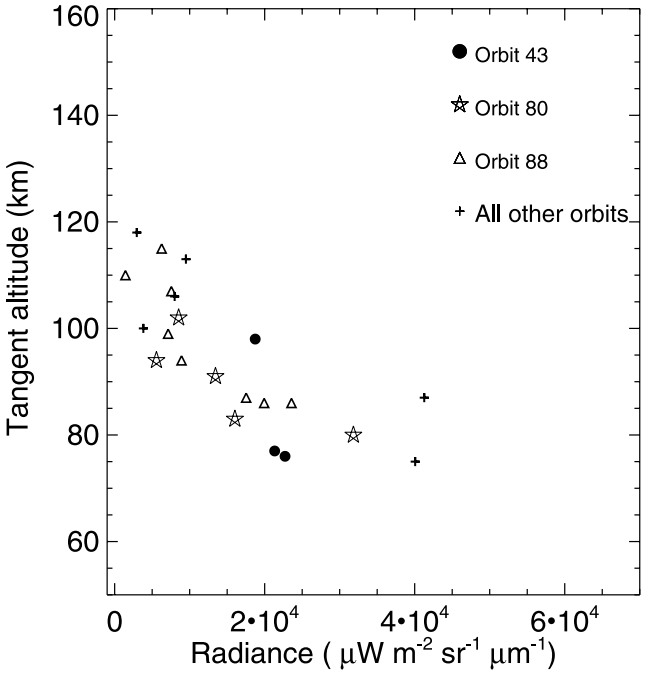

Figure 7. Vertical distribution or V-H radiances at a central wavelength of the 4.7-μm band of CO. Orbits and symbols as in Figure 3. See section 2.3.3.

CO_2 bands system. The vertical lines correspond to the actual pointing of each pixel, similarly to Figure 2. We will build similar maps with V-M data but from apoapsis observations, in the next section.

[32] Two strong variations are observed in the radiances, one along the vertical axis and the other along the horizontal, and both can be explained by the non-LTE model. Considering first the vertical, a peak emission is observed, in the lower thermosphere, 110–120 km. As the SZA varies along the track (from 70° to nighttime), the peak intensity, and the whole profile, decrease. This is predicted by the non-LTE model and this data set offers a perfect benchmark for a quantitative validation of the model; a work which is in progress.

[33] This is the first time that maps of IR radiation with this geometrical resolution are obtained in the Venus upper atmosphere. In order to illustrate more clearly such a resolution, we constructed a vertical profile with data from a single slit view, that indicated with an arrow in Figure 8. They are shown in Figure 9 (right), at three wavelengths. A log scale is used for the radiances, to confirm that a good signal to noise is achieved even at 160 km from one single spectrum. These data correspond to SZA $\sim$ 75°–80°, a value typical of daytime observations at high latitudes. The altitude of the peak is maximum in the center of the band, at 4.32 μm, and it is lower in the wings, at 4.25 and 4.40 μm, according to model expectations. Figure 9 (left) shows three V-M spectra at three tangent altitudes. The spectral resolution is lower than V-H, but the change in the overall shape of the band with altitude is clearly observed, as discussed in the previous section. We have also tried to build up maps of radiances in the 2.7-μm and 4.7-μm region. Unfortunately such V-M maps are very noisy at all altitudes, contain a very strong component of scattering up to 90 km, and are not further studied here.

2.5. VIRTIS-M Maps and Profiles During Apoapsis

[34] V-M observations from the apocenter of the Venus Express orbit are good examples to show the large potential of an imaging instrument like V-M for mapping large portions of the Venus disk. However, some images also contain information about atmospheric limb emissions, and

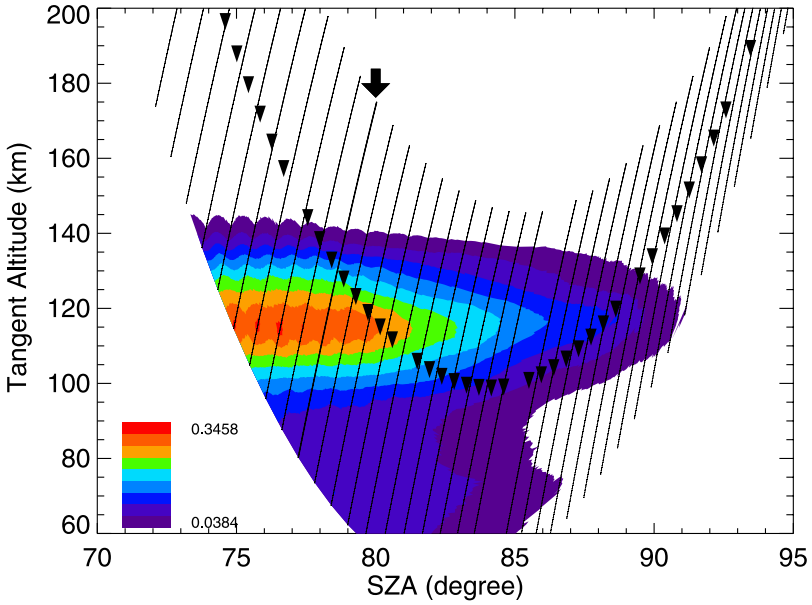

Figure 8. Map of V-M radiances from periapsis (orbit 43) at 4.32 μm versus SZA and tangent altitude. The color code ranges from 0.03 to 0.34 μW m^{-2} sr^{-1} μm^{-1}. Each line corresponds to a column of pixels along the V-M slit. V-H data for the same orbit are overplotted (triangles). The arrow indicates the column of pixels from which the vertical profiles in Figure 9 have been extracted.

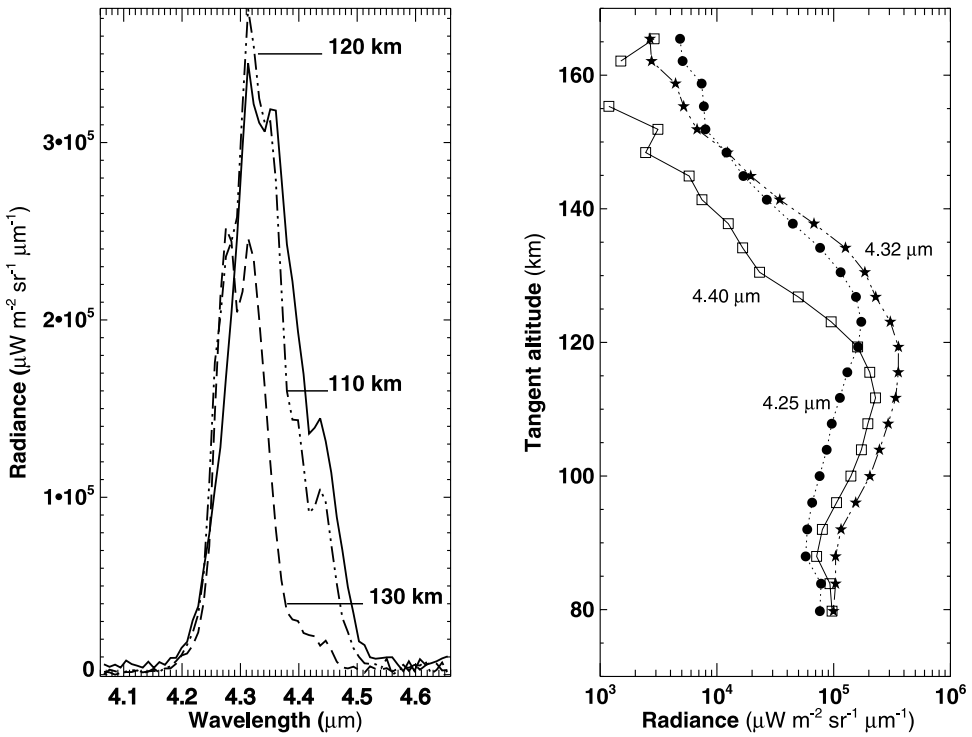

Figure 9. V-M spectra and profiles at 4.3 μm from periapsis, orbit 43. (left) Spectra at three different altitudes, as indicated. (right) Profiles at three wavelengths extracted from the pixels indicated in Figure 8. See section 2.4 for details.

allowed us to extract vertical profiles with an excellent vertical resolution.

2.5.1. 2-D Images From Apoapsis

[35] Figure 10 shows a map of V-M radiances at 4.32 μm, built up with the data from three consecutive qubes or V-M images (2, 1, and 0) of orbit 25, all of them acquired from apoapsis, at about 66,000 km from the center of Venus [*Svedhem et al.*, 2007]. The instrument takes about 10 min to take every qube, or image, before the satellite pointing switches to the next. The three images coincide with the data qubes shown in Figure 1a. The current map looks very different for two main reasons. First, now we are plotting

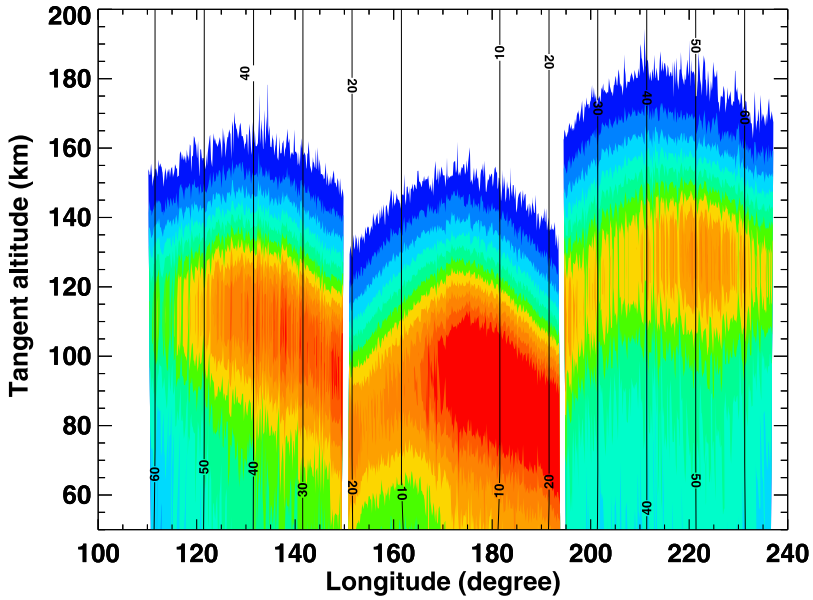

Figure 10. Maps of V-M limb radiances at 4.32 μm from apoapsis, from the three qubes of orbit 25 shown in Figure 1, as a function of tangent altitude and longitude. Vertical lines indicate SZA in degrees. Color scale is given in Figure 11.

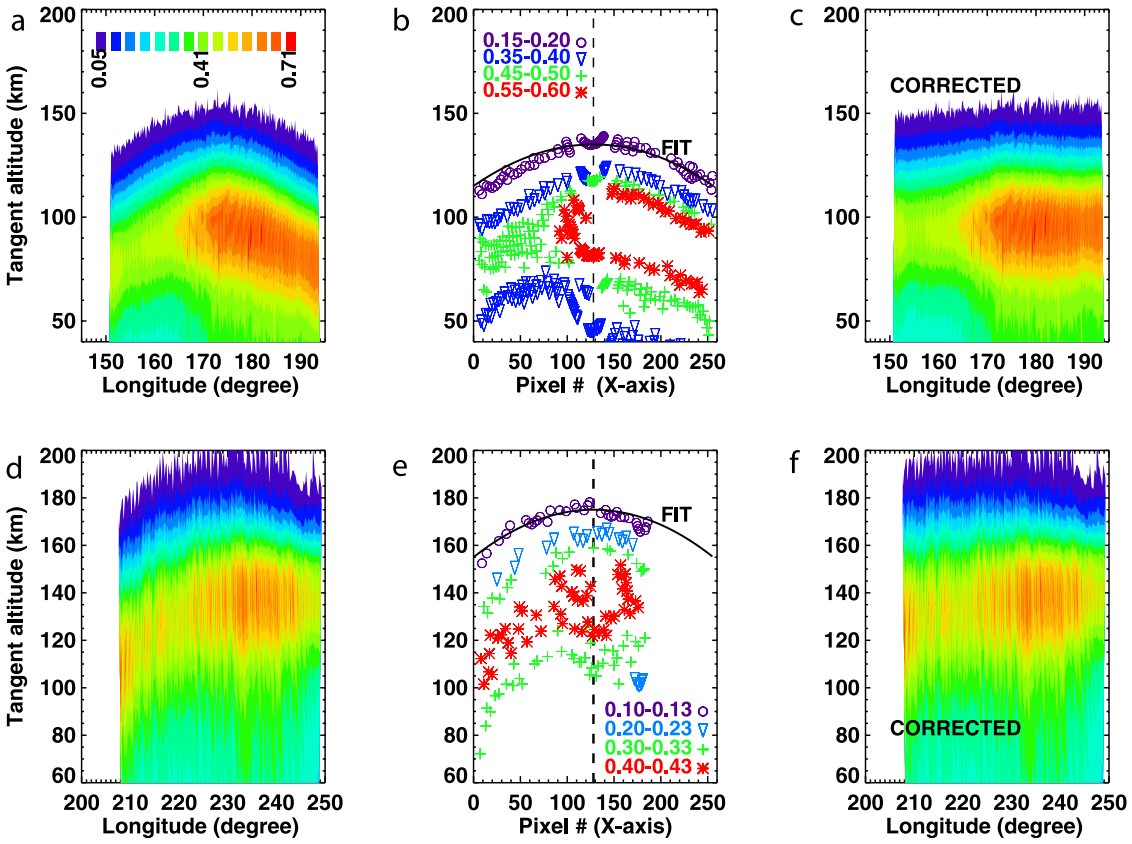

Figure 11. Smiling effect in V-M images from apoapsis and its correction for two cases: (top) qube 1 of orbit 25 and (bottom) qube 0 of orbit 29. (left) Original map of radiances at 4.32 μm. (middle) Location of pixels with radiance between the ranges indicated, and fit of a parabolic line to the cloud of pixels. (right) Corrected maps. See section 2.5.2 for details.

just the portion of the image which corresponds to actual limb sounding, i.e., tangent altitudes above about 60 km. And second, instead of pixel number, in Figure 10 we used altitude above the surface for the y axis, and a geographical parameter, longitude, in the x axis. Since the latitude is almost constant for all these limb data, Figure 10 represents a geometrically realistic view of such altitude-longitude cross section of the Venus upper atmosphere.

[36] Although the data acquisition and the image construction are different, this map is similar to the map from periapsis shown in Figure 8. Again, we observe a strong emission in the lower thermosphere, with a peak around 110–120 km. Also a large variation is observed in the horizontal axis. The SZA variation is, however, very small in each of the three qubes/images shown in Figure 10. Therefore, the horizontal variation may be of a different nature than that seen in the periapsis case, and might indicate a real atmospheric variability.

[37] However, extreme care is required before such an interpretation. The observations are taken from very far away, in a geometry which the instrument was not optimized for limb sounding; the data might contain some geometrical effects. First of all, these maps contain what appears to be a systematic bending of the radiances in the central part of the image. This bump has also been observed at other wavelengths, qubes, and dates, and it seems to be systematic. It is specially apparent in the uppermost layers. A second problem is shown by the sharp change in radiance between adjacent qubes. The three qubes shown here were taken with some minutes apart, and there is no obvious physical reason to expect changes of that magnitude between them. Investigation of these instrumental effects is ongoing. A likely explanation for the "smiling effect" is discussed in the next section. A probable cause for the second problem could be some flat field effect not yet identified.

2.5.2. Geometrical Correction of V-M Images

[38] The apparent bending observed in Figure 10 is of the order of 20 km, precisely the vertical resolution per pixel from the apoapsis, in other words, this error is within the size of one pixel. Although we cannot rule out small variations of the spacecraft pointing, the effect may be due to a slight bending of the V-M slit. This "smiling effect," which cannot be avoided, is of special importance for this limb sounding. Fortunately, some correction is possible, precisely by using these limb non-LTE emissions. We basically used two theoretical predictions of these emissions: first their strong decrease with tangent altitude, and second their variation with SZA, as explained below. The idea is to fit the bending observed with a simple function and then use that function to replot the radiances. We illustrate two examples of such a correction in Figure 11.

[39] Figures 11a and 11d show two different V-M images, those for orbit 25 (15 May 2006), qube 1 and orbit 29

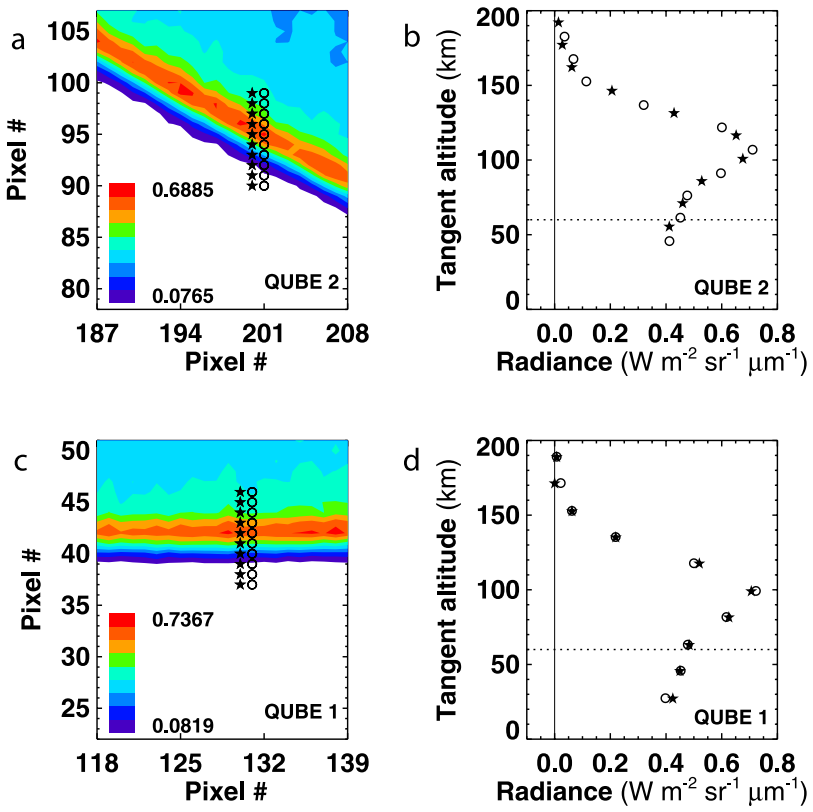

Figure 12. Vertical profiles of V-M radiance at (right) 4.33 μm after combining the (left) rows of pixels. (top) Qube 2 of orbit 25. (bottom) Qube 1.

(19 May 2006), qube 2; these are the original maps to transform. The correction has to be applied to them on a pixel basis, as we will assume it to be symmetric around the central pixel of the frame 128. Then we have selected all those pixels with radiances within a small bracket of values; they are marked with crosses in Figures 11b and 11e. According to the non-LTE model, if the atmospheric densities and the SZA illumination do not change very much, a given limb radiance corresponds to a given tangent altitude. Actually, this is the reason why we discovered this smiling effect. We can observe how the crosses marking the 0.15–0.20 radiance interval indicate a bending approximately symmetric around pixel 128. We fit a simple parabolic function to this cloud of pixels, and used it to correct for the tangent altitude of all the 256 pixels in each row of the frame. A perfect fit cannot be obtained owing to the different sources of error, which produce some dispersion in the measurements. In addition, the cloud of data does not present a random distribution but a peculiar dispersion produced by the particular geometry of the observations, which is specific for each qube. Some atmospheric variability cannot be ruled out either. For these reasons, we aim here at a first-order correction. Let us notice, also, that it will be difficult to find a single fit function with matches all the radiance intervals of all the orbits and qubes. In our example, the radiance maps resulting after the correction are shown in Figures 11c and 11f. The bending of about 20 km is greatly reduced. This correction function introduces some uncertainty in the absolute pointing altitudes. In the center of the frame, around pixel 128, the correction is very small, but the pointing may be inaccurate by around 5 km for the pixels at the extremes of the V-M frame. Still, we believe that the corrected images can be used for scientific studies, like atmospheric variability, possible dependence of the emissions on non-LTE parameters, etc, which would be impossible without this geometrical correction. In the VIRTIS team we are considering the implementation of this procedure in future operational processing.

2.5.3. Vertical Profiles From V-M 2-D Images

[40] Lets analyze now the vertical profiles of radiance from the limb that can be obtained from these V-M images at the apoapsis. As an example, Figure 12 shows two vertical profiles extracted from two different data qubes, already shown in Figure 1, qubes 2 and 1 of orbit 25. The profiles, at the wavelength of 4.32 μm, are shown on the right, while on the left we plot a small portion of the qube/image and marked the precise pixels used to build the profiles. The portion of the Venus disk selected corresponds to an almost constant solar illumination, with a small change of SZA, from 10° to 20°. To build up the profiles, we considered two adjacent sets of 10 pixels, taken at the same time, from two adjacent rows of the V-M frame. The selected pixels are pointing at varying altitudes, from the planet's surface up to the Venus thermosphere, with a vertical resolution around 15 km, and symbols in Figure 12 just point to the center of each pixel. If the orientation of the limb of Venus is optimum, as we can see in Figures 12a and 12b, a very good altitude resolution can be achieved by mixing adjacent pixels; otherwise, the gain in vertical resolution is lower or nonexistent. The improvement of

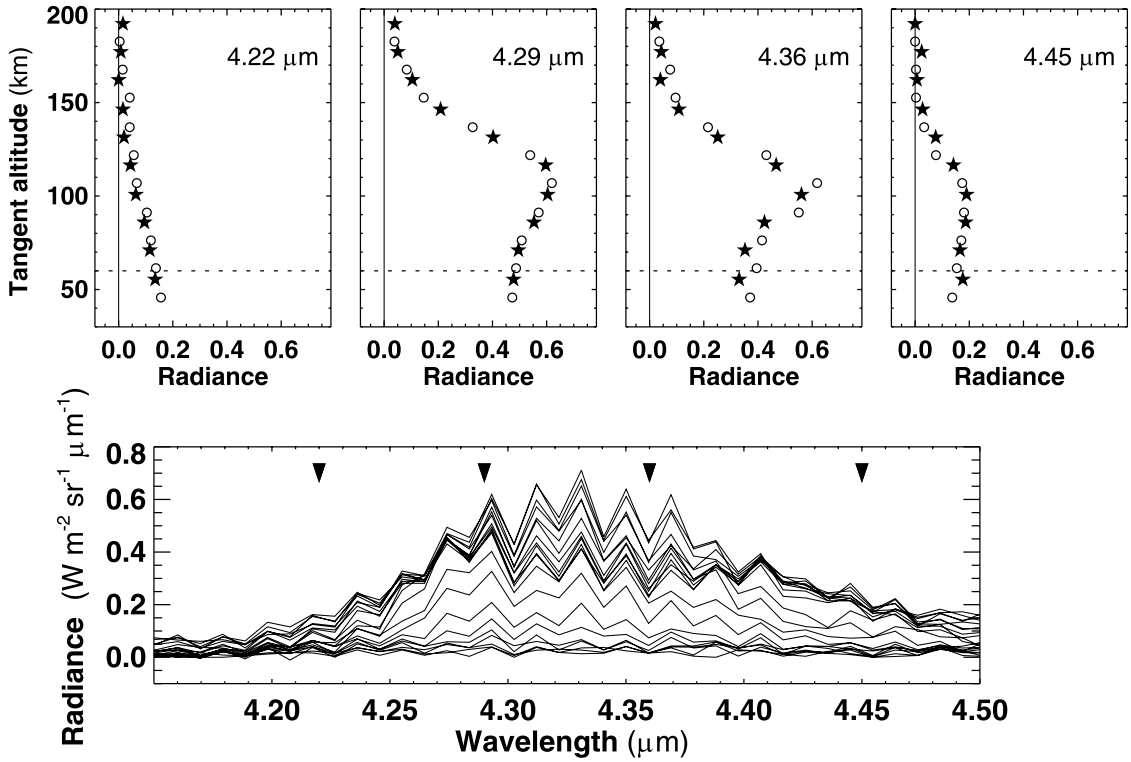

Figure 13. (top) Vertical profiles of V-M radiances at four wavelengths for qube 2, orbit 25. (bottom) Spectra of the 20 pixels composing the vertical profiles shown on the top; they belong to 2 adjacent rows of pixels, marked with stars and circles as in Figure 12. Four triangles mark the wavelengths of the four vertical profiles.

the vertical resolution is at the expense of losing horizontal resolution, obviously.

[41] Other four vertical profiles are shown in Figure 13 (top), obtained from the same rows of pixels in the top of Figure 12 but at four different wavelengths in the 4.3-μm region. The wavelength values are marked in Figure 13 (bottom), which shows the 20 spectra considered. We can get a lot of useful information about the non-LTE emissions from an image like this, since it combines spectral and vertical variations. For instance, the peak altitude is shown to vary with wavelength, being higher at 4.29 μm or 4.33 μm (see Figure 12) than in the wings of the band. This was predicted by the non-LTE model, and was observed also in periapsis observations. Although the qualitative behavior seems to agree with the model, the vertical profile at 4.45 μm does not coincide with the model, but this suggests a much lower emission compared with the center of the band. We think this may be solved by increasing the number of weak CO_2 bands in the non-LTE model, a task for a forthcoming revision of the non-LTE model that we are currently undertaking.

[42] A systematic problem in V-M data can be noticed in Figure 13 (bottom). There seems to be an oscillation in the spectral domain, with high and low values of intensity from one spectral point to the next. We checked that this "odd-even effect" is present at all VM near-IR wavelengths, from 2 to 5 μm, and it amounts to about 0.05 radiance units in Figure 13, or 50,000 μW m^{-2} sr^{-1} μm^{-1}, which is about 10 times larger than the measurement noise. The technical cause of the odd-even seems to be an asymmetry of the Read-Out Integrated Circuit (ROIC) of the Focal Plane Array (FPA) of the instrument; see *Coradini et al.* [1998] for a more detailed description of the instrument. In particular, there is an asymmetry in the clock feedthrough and the unit cells between pixels in odd columns and pixels in even columns, which causes some differences in gain and offset. Most part of this effect is corrected through the radiometric calibration where the responsivity of each pixel is taken into account. However, there seems to be also a problem of the offset/reset being dependent with the signal, which makes the difference of the odd-even effect bigger for extreme conditions, which is the case of very high signals or very low exposure times. During periapsis, for example, the exposure time is about 10 times larger than in apoapsis. This is the reason why the odd-even effect is much smaller (at or below the noise level) in Figure 9. Let us recall that odd-even effects are common in imaging spectrometers, in the spectral or spatial domains [*Moutou et al.*, 2003; *Siebenmorgen et al.*, 2007]. We will return to this point in the next section.

3. Validation Analysis

[43] Validation analysis traditionally comprises direct comparisons with independent observations. This is not possible with our VIRTIS limb data, although eventually, some indirect comparisons with related measurements by other Venus Express instrument, like neutral densities from VERA and SPICAV, will be possible. At this stage, however, our analysis focused on other aspects. These include (1) internal consistency tests and comparison with averages,

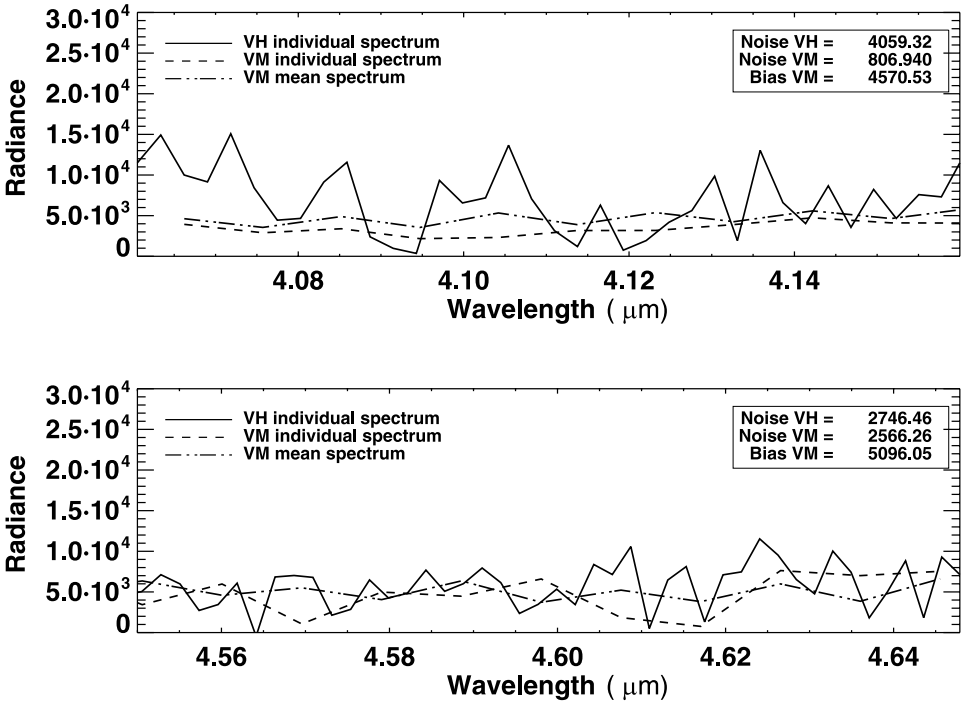

Figure 14. V-H and V-M noise and bias in a selection of spectra around 4.3 μm from periapsis, at a tangent altitude of 118 km. Radiance units are μW m^{-2} sr^{-1} μm^{-1}. See section 3.1 for further details.

(2) estimation of noise/data quality, (3) cross correlation between the two VIRTIS signals, (4) qualitative comparisons with theoretical non-LTE models, and (5) examination of the repeatability and variability of the measurements. The goal is to characterize the behavior of the VIRTIS instrument, to confirm that the measurements are physically meaningful, and to detect potential bias or systematic errors. The most important of these analysis, and their conclusions, are presented next.

3.1. Noise and Bias in V-H and V-M

[44] One of our basic objectives was to evaluate the measurement noise in orbit, in the spectral ranges and emissions of our interest, to compare it with the nominal one obtained by ground calibration, and at the same time, to analyze possible systematic effects. A first step was the examination of individual spectra for the orbits with limb data. A second task was to average homogeneous sets of data, considering appropriate boxes in SZA and tangent altitude, and to calculate their mean radiance and dispersion.

[45] For the evaluation of the noise level and the bias in the 4.3-μm region, we looked at the two wings of this CO_2 system of bands, shortward and longward of 4.20 and 4.50 μm, and at altitudes where no significant emission is expected there. The mean radiance of each spectrum can be considered as the bias, and its standard deviation (SD) as an estimation of the noise. An example for orbit 43 (periapsis) is shown in Figure 14, where two individual spectra are shown, one from V-H and a nearby one from V-M. The tangent altitude is around 120 km.

[46] Regarding V-H, the noise values obtained for this particular example are similar in the left and right wings of the band, and slightly lower than the nominal noise of 5000 μW m^{-2} sr^{-1} μm^{-1}. We have evaluated these values for a diverse set of spectra, for different orbits, solar illumination conditions and tangent altitudes, and have found that they are basically constant up to orbit 47 (7 June 2006) and decrease to about half those values after orbit 79 (8 July 2006). This is probably related to the spacecraft thermal evolution along the mission, with higher noise levels at the beginning of the mission, when the cold box temperature was higher.

[47] Regarding the V-M data, the noise in this example is also lower than the nominal value, although there is a significant difference between the left and right wings of the band. Regarding its bias, the availability of a large number of spectra from V-M at a given position, allows us to estimate it for a close subset of pixels. In Figure 14 we added another spectrum, that obtained by averaging 25 V-M pixels/spectra within a small range of tangent altitudes (118–120 km) and SZA (78°–81°) around the V-M spectrum selected. The mean value coincides well with the bias obtained from one single spectrum.

[48] Similar noise and bias analyses for V-M at apoapsis are difficult at present owing to the large odd-even effect mentioned above, much larger than those parameters. In fact, the averaged V-M spectrum in Figure 14 shows more clearly such oscillation in the intensity than one single spectrum. This effect has a magnitude (amplitude between peaks) of about 2000 μW m^{-2} sr^{-1} μm^{-1}, of the order of the noise. The V-M calibration group of the VIRTIS team is currently working on this point, in order to reduce its impact on apoapsis data.

3.2. Correlation Between V-H and V-M Spectra

[49] There is a small number of observations in the Spectral Mode which correspond to the special Tangential Limb sounding, with simultaneous measurements of V-H

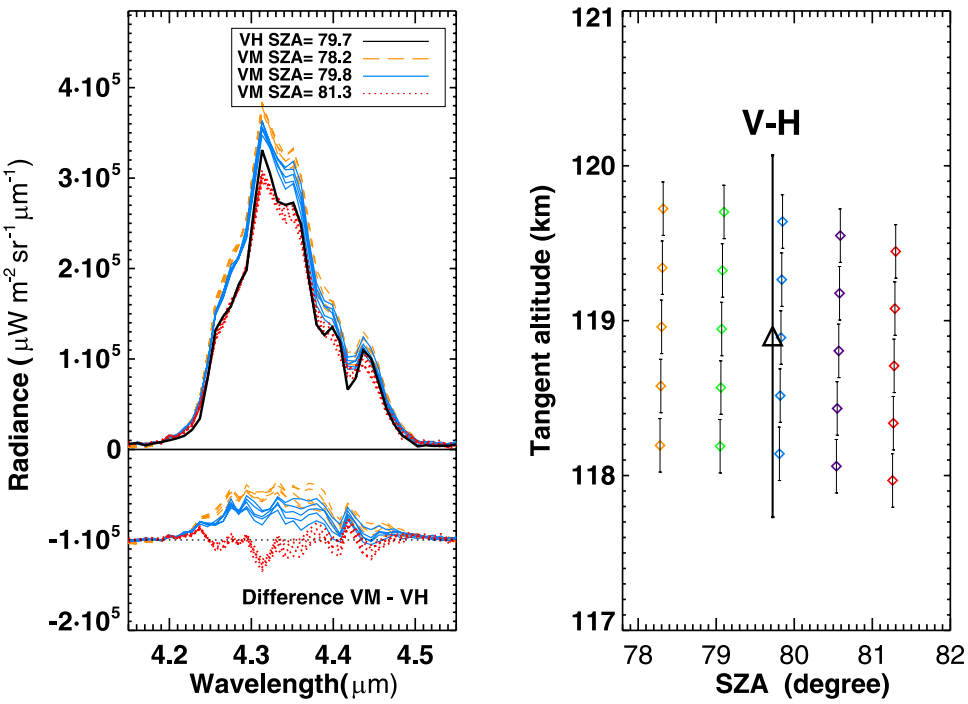

Figure 15. Correlation between V-M and V-H spectra taken during periapsis, orbit 43. (right) Location in tangent altitude and SZA, with approximate size of the V-H and V-M field of view. (left) Spectra of the 15 selected V-M pixels, those with SZA of 78.2°, 79.8°, and 81.3°, and of the V-H spectrum (convolved to V-M spectral resolution). Differences between V-H and V-M spectra are also plotted below. See section 3.2 for further details.

and V-M. The proximity to the planet during periapsis, allows for a precise geographical collocation of these profiles, and therefore, permits a specially appropriate comparison between them. Orbit 43 offers one example, and Figure 8 shows how close V-M and V-H measurements can be. Figure 15 shows a number of VM spectra close to one particular V-H spectrum, obtained at that orbit, around SZA = 80° and 119 km tangent altitude. Five adjacent slit images were considered, with five pixels on each. The vertical size of the pixel's FOV, about 300 m for V-M and 2 km for V-H, is shown on the right. On the left we plot 15 of the VM spectra, those from the groups at SZA of 78.2°, 79.9°, and 81.3°, and compare them with the V-H spectrum. This was degraded/convolved to the lower spectral resolution of V-M for the comparison. The shape of the whole CO_2 band is very well reproduced by all of them. We think the overall comparison seems fairly good, given the dispersion among the 15 V-M spectra plotted. These present, first of all, a small dispersion within each group, which is similar or slightly larger than typical noise and bias levels. In addition there is a small variation between the three groups, significantly larger than the noise, which is surely due to the small SZA difference between them; the radiance at larger SZA being smaller, as expected. Comparing the V-H spectrum with its closest V-M group of spectra, there is a small shift between them, of about 40,000 μW m^{-2} sr^{-1} μm^{-1} around the peak at 4.33 μm, larger than the noise and bias of both, V-H and V-M. However, this difference is only a factor 2 larger than the SD of this particular group of V-M data, and equivalent to a small fraction of a degree in SZA. This gives us a good level of confidence on both signals.

[50] The emission at 2.7 μm can also be used to test the V-H and V-M agreement. Although the number of spectra with good signal is very limited, we found some spectra in the orbit 43 which are useful for the present discussion. They are shown in Figure 16 and correspond to SZA = 80° approximately. Figure 16 (top) shows vertical profiles at three wavelengths in the 2.7 μm spectral region and show a neat altitude variation, with a clear peak around 115–120 km. This was predicted by the LVEA model. Figure 16 (bottom) shows the mean and standard deviation of a set of 15 V-M spectra, at altitudes around 120 km. The error bars of individual V-H and V-M are slightly larger than the nominal values, and they have been omitted in Figure 16. The agreement between V-H (convolved to V-M resolution) and V-M is good within error bars; there may be a slight mismatch around 2.8 μm but the data seem noisier there. Moreover, this emission is lower and noisier than that shown in Figure 5, at all wavelengths, since the solar excitation is lower now. We performed a simulation with the non-LTE model, also shown in Figure 16, for the same solar illumination conditions. The agreement is very encouraging, although the model seems to overestimate the radiance; this is due to the specific atmosphere structure assumed in the simulation, and therefore is of no relevance in this analysis.

[51] Related to this correlation, we investigated the correlation between different V-H spectra, wherever they can be collocated. The amount of V-H spectra is not large, but we identified a couple of interesting correspondences between spectra with good S/N ratio. On Figure 17 (left), they correspond to four consecutive V-H measurements (acquisition 84 to 87) obtained at the closest approach to Venus

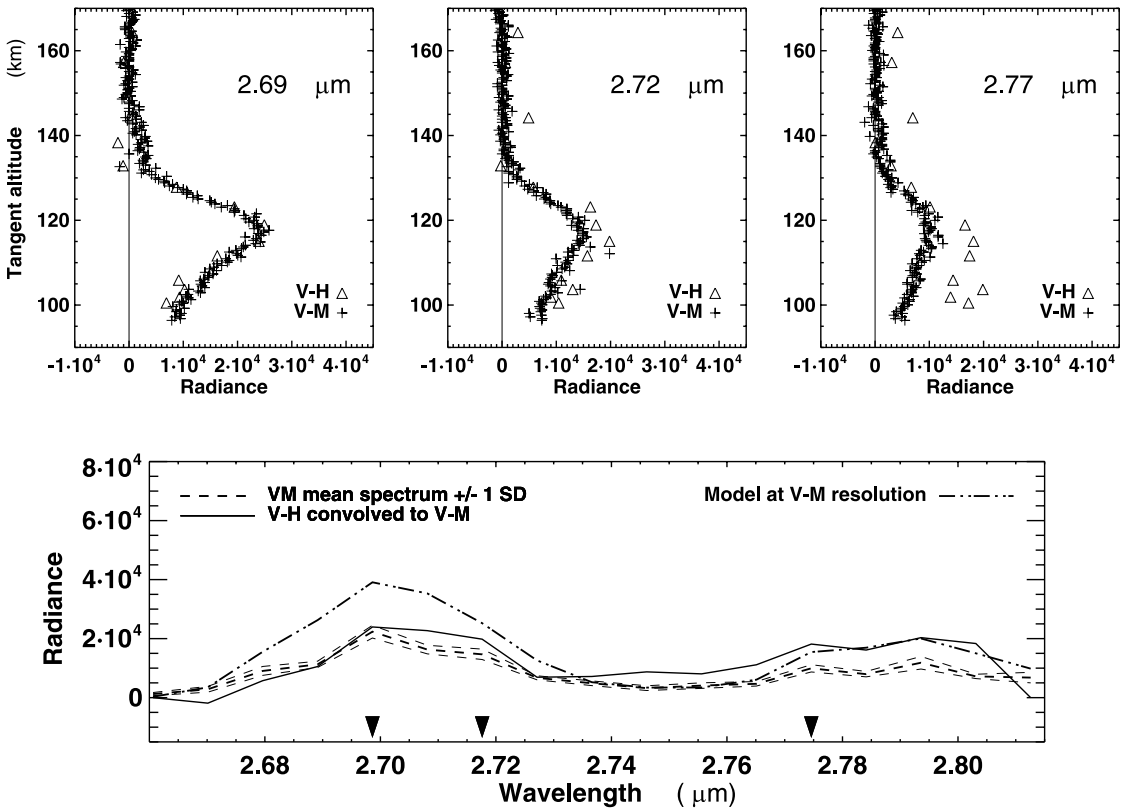

Figure 16. (top) Vertical profiles of V-H and V-M radiances at three wavelengths in the 2.7 μm for qube 0, orbit 43 and SZA around 80°. Triangles and crosses mark V-H and V-M data, respectively. (bottom) One V-H spectrum, convolved to V-M resolution (solid line) and comparison with the mean of 15 V-M spectra (dashed lines), from the data composing the vertical profile in the top, at a tangent altitude of 120 km. The dashed-dotted line represents a model simulation. Radiance units are μW m^{-2} sr^{-1} μm^{-1} in both the top and bottom. Three triangles in the bottom indicate the wavelengths of the three vertical profiles.

during orbit 43, and point to the lowest tangent altitudes for this orbit, around 99 km (as indicated in the picture) and around SZA = 83° (see Figure 8). The geometrical distance along the track of the satellite between the spectra 84 and 87 is about 250 km, and they correspond to latitudes of 73.0° and 71.8°, longitudes of 302° and 307°, respectively, and a difference in SZA of 1.4°. The four spectra are very similar, with differences of the order of the noise at almost all wavelengths, except in the central region. Around 4.3 μm there is a clear trend, from 84 to 87, the last one being about 30,000 μW m^{-2} sr^{-1} μm^{-1} lower than the former. We think, again, that this is due to SZA changes; close to the terminator small changes in SZA produce noticeable variations in the solar pumping of the CO_2 vibrational states. This reflects small changes in the atmospheric structure between those four locations.

[52] Figure 17 (right) presents another two V-H spectra, very closely located to each other, both at a latitude of 77.27°S and longitudes of 257.8°E and 260.8°E, respectively, but obtained 2 days apart, on orbits 40 and 42. Their tangent altitudes and SZA are also very close, at 108.4 and 107.8 km, and 82.7° and 82.3°, respectively. Their noise and bias levels are below 5000 μW m^{-2} sr^{-1} μm^{-1} and 8000 μW m^{-2} sr^{-1} μm^{-1}, respectively. It is surprising the excellent agreement between them in the overall shape and in the wings of the band; there is only a small difference, in the central portions of the CO_2 emission, with the spectrum of orbit 42 slightly larger than the other and the noise. Again, the small SZA differences is a possible candidate for the observed difference. This points, once more, to a relatively calm and stable atmospheric structure, fully repeatable in times scales of 2 days, at least in this case. It would be interesting to explore further coincidences of this type in future measurements of V-H, since the number of them available to date is small (see Figure 3).

3.3. Comparisons With a Non-LTE Model

[53] As discussed above, we have used in this work the non-LTE model of the Venus atmosphere developed at the Instituto de Astrofísica de Andalucía/CSIC, in Granada [*Roldán et al.*, 2000; *López-Valverde et al.*, 2007], to perform a small number of simulations. These simulations and those reported by LVEA have guided most of the analysis presented in previous sections. From these comparisons we found a good overall agreement with the predictions of the spectral shape of V-H and V-M data (Figures 4, 9, and 17), and with the altitude profiles of the radiances in the central part of the 4.3-μm band (Figures 4 and 9). Also the SZA variation of the peak radiance (Figures 8 and 15) qualitatively agrees with expectations. The vertical profiles of the CO_2 emission shown in Figures 9 and 13 do agree qualitatively with those of LVEA but a quantitative fit

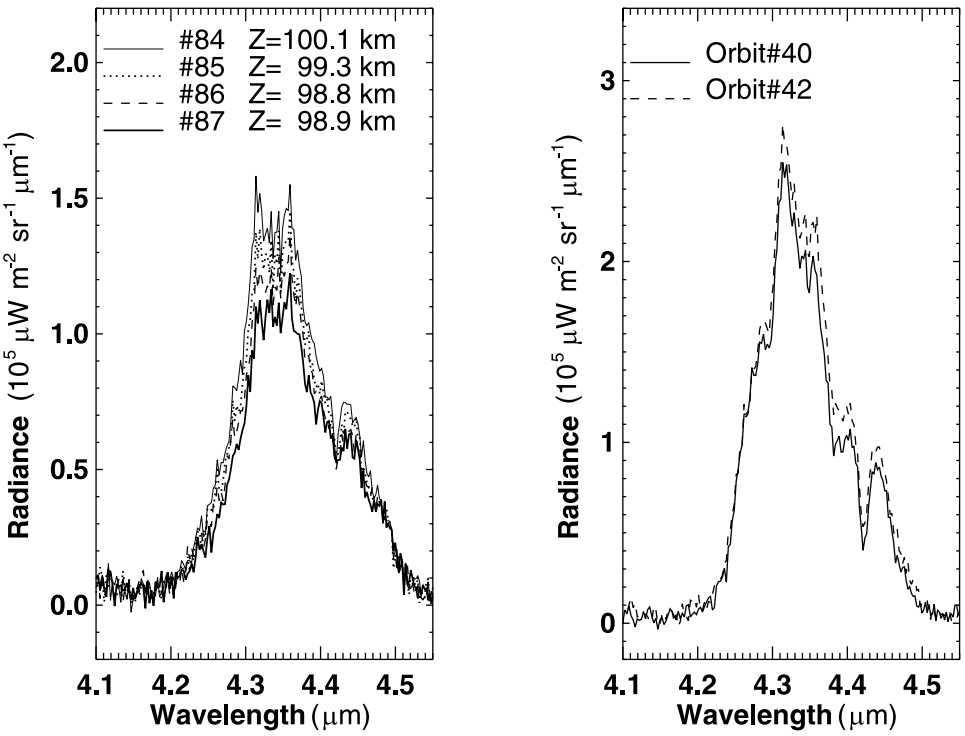

Figure 17. Geographical coincidences between different V-H spectra. (left) Four spectra from orbit 43, around 99 km. (right) Example of two spectra taken at very close points but 2 days apart. Variations attributable to SZA changes. See section 3.2 for details.

would be desirable and future work should focus on this aspect and exploit such fit, once the weak bands required are implemented into the model. Other non-LTE emissions predicted by LVEA have also been examined, detected and compared with the model. Figures 5 and 16 show simulations of the CO_2 2.7 μm bands for a given reference atmosphere; they indicate a good agreement in the spectral shape of the bands, and for both V-H and V-M spectral resolutions. Although these data are noisy, the main features are captured by the model, and the vertical profiles are also in agreement, with similar altitudes of the peak emission in the data and in the model. The absolute emission, as it happens with the 4.3 μm bands, is not considered in this comparison, since it depends on the actual atmospheric structure assumed in the non-LTE model. The third non-LTE emission detected and studied in this work, that of CO, contains a first hot component not simulated yet by the non-LTE model.

[54] Let us highlight here some other results which, either were not predicted or seem to pose interesting challenges to the theoretical modeling. One of them is the intensity in the longer wavelength wing of the 4.3 μm band, where contributions from weak, isotopic and hot transitions are expected. The predictions by LVEA produce a relatively minor contribution of that band's wings compared to the central band, but the VIRTIS spectra shown in Figures 4 and 9 indicate a more significant contribution. The model surely needs a larger number of CO_2 bands in this spectral region. Such a model extension is underway.

[55] Certainly, another extension of the non-LTE model is needed to include the first hot band of carbon monoxide, CO(2-1), in order to study the spectra shown in Figure 6. This is also a minor band compared to the strongest fundamental transition, but it seems to be highly excited by direct solar radiation, like the weaker transitions of CO_2 discussed above. As discussed in section 2.3.3, a proper simulation of the CO emission lines will be very valuable for the derivation of rotational temperatures. These could be obtained from this band's structure, but only after fitting a theoretical model which permits small radiance errors in the line peaks. This is the only molecular band detected by VIRTIS in this infrared portion of the spectrum with well isolated lines, and is therefore a very interesting data set.

4. Conclusions and Future Work

[56] VIRTIS on Venus Express is an innovative instrument which, combining imaging and spectroscopy in the near infrared, is obtaining very exciting new data on the upper atmosphere of Venus. We have analyzed the limb measurements taken by VIRTIS in the regions from 4 μm to 5 μm and around 2.7μm from both, the periapsis and the apoapsis of the Venus Express orbit, and in the two signals, V-H at high spectral resolution, and V-M at a lower resolution. We have focused in this work on a subset of VIRTIS data, which includes limb measurements with V-H taken at the periapsis from orbits 23 (13 May 2006) to 127 (25 August 2006), and a small sample of V-M data qubes between orbits 23 (13 May 2006) and 295 (10 February 2007). Extension of the analysis presented here to the rest of the data is ongoing.

[57] We clearly identified the strong emission by CO_2 at 4.3 μm in the upper mesosphere and lower thermosphere, and of the first hot band of CO at 4.7 μm in the upper

mesosphere. Individual spectra show good signal to noise up to above 160 km in the case of CO_2, and up to about 120 km in the case of CO. Single spectra show noise values slightly below the value expected from ground calibration, and a small bias too. We also showed that the V-H spectral resolution is good enough for a number of tests of our non-LTE models. The spectral resolution of V-M is lower, however the vertical resolution is much better from V-M data. During periapsis this is typically 300 m for a single row of pixels, while from apoapsis, the grouping of V-M adjacent rows of data permits a resolution at least two to three times better than the FOV of individual pixels, depending on the geometry of the V-M images and on the relative orientation of the limb of Venus. These observations characterize the Venus atmosphere directly, since they will permit to calculate densities and temperatures from measurements, and also indirectly, because they can give information about the collisional processes, energy transfer and the upper atmosphere energy balance, after a more detailed comparison with a non-LTE model.

[58] The variability observed by VIRTIS and mentioned previously by *Drossart et al.* [2007a] have been confirmed and analyzed here for the first time with this new and extended data set. The maps studied in this paper permit to describe altitude variations at several wavelengths, variations with SZA, and the detailed spectral shape of the CO and CO_2 bands. Actually, the good agreement between model and data, on the basic non-LTE features, indicates that our current understanding of the physical processes in the upper atmosphere is essentially correct. All these results will be perfect tests for future non-LTE models, and suggestions for more detailed future comparisons are given in section 3.3. We foresee that such detailed comparisons, specially of the shape of the V-H emissions, can give us information about non-LTE collisional parameters in the upper mesosphere and lower thermosphere, where these processes are specially relevant. Also, comparisons between spectra at similar conditions but obtained with a span of 2 days, and between data more than 200 km apart, show very good matches, which indicates a good behavior of VIRTIS. When applied to a future and extended data set, similar comparisons may supply interesting information about atmospheric variability in the lower thermosphere. The high density of points in the limb in some maps during periapsis offer excellent chances for derivation of density maps in the thermosphere. Such density profiles are foreseen to be obtained by a rigorous "retrieval" process which uses inversion techniques under non-LTE conditions, an exercise similar to other upper atmosphere experiment on Earth, like the MIPAS/Envisat data analysis [*Funke et al.*, 2005]. Densities of CO would be derived in a limited altitude range (90–120 km) owing to the low signal of the CO 4.7 μm emission (see section 2.3.3). However, densities of CO_2 can be derived in principle in a wider altitude range. Nevertheless, the accuracy of such derivation will depend on a sensitivity study to be performed with the revised non-LTE model. Limb views from V-M during apoapsis should also be very useful for density retrievals, although they are affected at present from a "smiling effect" which deforms the actual emission field by about 20 km, approximately the size of the projected FOV of one pixel. We showed how the non-LTE model has been essential to detect this effect which could be reduced in future processing thanks to a correction technique using these CO_2 non-LTE emission. These V-M data from apoapsis are also affected by a large odd-even effect, about 10 times larger than the noise level. During periapsis this effect is below noise due to the much larger exposure time there. This aspect requires further work within the VIRTIS team in the future.

[59] The study of the first hot CO(2-1) emission is also very promising, since the rotational structure is resolved and it can therefore be used to derive rotational temperatures in the upper mesosphere. This will be confined to daytime and to the altitude range 90–120 km, where such signal is strongest. This derivation does not require a full non-LTE retrieval but a fit of the shape of the CO emission band with the model, as explained in section 2.3.3. At present, uncertainties in individual lines of a CO spectrum produce very large temperature errors. Comparisons with temperatures obtained from ground-based measurements of these bands [*Crovisier et al.*, 2006] will also be interesting, as a validation exercise of these data and in order to future check the non-LTE models.

[60] VIRTIS/Venus Express will continue acquiring new data at least until 2009. The exploration of the new data and their analysis will continue, hopefully with a version of the non-LTE model extended to weaker bands, and with better understanding of some of the current uncertainties in the data that we highlighted here. The application of retrieval techniques and systematic search for atmospheric variability, makes the VIRTIS observations a very promising data set for studying the non-LTE processes and the structure of the upper atmosphere of Venus.

[61] **Acknowledgments.** We thank the space agencies ASI and CNES for their support. The work of the IAA-CSIC team has been carried out under project ESP2004-01556 and was partially funded by the project AYA2008-03498/ESP of the Spanish Ministery of Science and Innovation and by EC-FEDER funds. GG has been partially supported by a fellowship from Spanish National Research Council (CSIC-JAE Program).

References

Bougher, S. W., D. M. Hunten, and R. G. Roble (1994), CO_2 cooling in terrestrial planet thermospheres, *J. Geophys. Res.*, *99*, 14,609–14,622.

Carlson, R. W., et al. (1991), Galileo infrared imaging spectroscopy measurements at Venus, *Science*, *253*, 1541–1548.

Carlson, R. W., P. R. Weissman, W. D. Smythe, and J. C. Mahoney (1992), Near-Infrared Mapping Spectrometer experiment on Galileo, *Space Sci. Rev.*, *60*, 457–502.

Coradini, A., F. Capaccioni, P. Drossart, A. Semery, G. Arnold, and U. Schade (1998), VIRTIS: An imaging spectrometer for the Rosetta mission, *Planet. Space Sci.*, *46*, 1291–1304.

Crovisier, J., E. Lellouch, C. de Bergh, J.-P. Maillard, B.L. Lutz, and B. Bèzard (2006), Carbon monoxide emissions at 4.7 μm from Venus' atmosphere, *Planet. Space Sci.*, *54*, 1398–1414, doi:10.1016/j.pss.2006.04.027.

de Bergh, C., J. Crovisier, B. L. Lutz, and J.-P. Maillard (1988), Detection of CO infrared emission lines in spectra of Venus, *Bull. Am. Astron. Soc.*, *20*, 831.

Deming, D., F. Espenak, D. Jennings, T. Kostiuk, M. Mumma, and D. Zipoy (1983), Observations of the 10-um natural laser emission from the mesosphere of Mars and Venus, *Icarus*, *55*, 347–355, doi:10.1016/0019-1035(83)90107-0.

Dickinson, R. E. (1972), Infrared radiative heating and cooling in the Venusian mesosphere: I. Global mean radiative equilibrium, *J. Atmos. Sci.*, *29*, 1531–1556.

Drossart, P., et al. (2007a), A dynamic upper atmosphere of Venus as revealed by VIRTIS on Venus Express, *Nature*, *450*, 641–645, doi:10.1038/nature06140.

Drossart, P., et al. (2007b), Scientific goals for the observation of Venus by Virtis on ESA/Venus Express mission, *Planet. Space Sci.*, *55*, 1653–1672, doi:10.1016/j.pss.2007.01.003.

European Space Agency (ESA) (2001), Venus Express: An orbiter for the study of the atmosphere, the plasma environment, and the surface of Venus, *Eur. Space Agency Sci. Tech. Rep., ESA STR 6*, 46 pp.

Formisano, V., A. Maturilli, M. Giuranna, E. D'Aversa, and M. A. Lopez-Valverde (2006), Observations of non-LTE emission at 4–5 microns with the Planetary Fourier Spectrometer aboard the Mars Express mission, *Icarus*, *182*, 51–67, doi:10.1016/j.icarus.2005.12.022.

Funke, B., et al. (2005), Retrieval of stratospheric NO_x from 5.3 and 6.2 μm nonlocal thermodynamic equilibrium emissions measured by Michelson Interferometer for Passive Atmospheric Sounding (MIPAS) on Envisat, *J. Geophys. Res.*, *110*, D09302, doi:10.1029/2004JD005225.

García, R., M. A. López-Valverde, P. Drossart, and G. Piccioni (2009), Gravity waves in Venus atmosphere revealed by CO_2 non-LTE emission, *J. Geophys. Res.*, doi:10.1029/2008JE003073, in press.

Gordiets, B. F., and V. I. Panchenko (1983), Non-equilibrium infrared emission and the natural laser effect in the Venus and Mars atmospheres, *Kosm. Issled.*, *21*, 929–939.

Hueso, R., A. Sánchez-Lavega, G. Piccioni, P. Drossart, J. C. Gèrard, I. Khatuntsev, L. Zasova, and A. Migliorini (2008), Morphology and dynamics of Venus oxygen airglow from Venus Express/Visible and Infrared Thermal Imaging Spectrometer observations, *J. Geophys. Res.*, *113*, E00B02, doi:10.1029/2008JE003081.

López-Puertas, M., and F. W. Taylor (2001), *Non-LTE Radiative Transfer in the Atmosphere*, *Ser. Atmos., Oceanic, Planet. Phys.*, vol. 3, World Sci., Singapore.

López-Valverde, M. A., and M. López-Puertas (1994), A non-local thermodynamic equilibrium radiative transfer model for infrared emission in the atmosphere of Mars: 2. Daytime populations of vibrational levels, *J. Geophys. Res.*, *99*, 13,117–13,132.

López-Valverde, M. A., M. López-Puertas, J. J. López-Moreno, V. Formisano, D.Grassi, A. Maturilli, E. Lellouch, and P. Drossart (2005), Analysis of CO_2 non-LTE emissions at 4.3 μm in the Martian atmosphere as observed by PFS/Mars Express and SWS/ISO, *Planet. Space Sci.*, *53*, 1079–1087, doi:10.1016/j.pss.2005.03.007.

López-Valverde, M. A., P. Drossart, R. Carlson, R. Mehlman, and M. Roos-Serote (2007), Non-LTE infrared observations at Venus: From NIMS/Galileo to VIRTIS/Venus Express, *Planet. Space Sci.*, *55*, 1757–1771, doi:10.1016/j.pss.2007.01.008.

Moutou, C., A. Coustenis, J. Schneider, D. Queloz, and M. Mayor (2003), Searching for helium in the exosphere of HD 209458b, *Astron. Astrophys.*, *405*, 341–348.

Piccioni, G., et al. (2006), VIRTIS: The Visible and Infrared Imaging Spectrometer, *Eur. Space Agency Spec. Publ.*, *ESA-SP 1295*, 1–27.

Roldán, C., M. A. López-Valverde, M. López-Puertas, and D. P. Edwards (2000), Non-LTE infrared emissions of CO_2 in the atmosphere of Venus, *Icarus*, *147*, 11–25, doi:10.1006/icar.2000.6432.

Roos-Serote, M., P. Drossart, Th. Encrenaz, E. Lellouch, R. W. Carlson, K. H. Baines, F. W. Taylor, and S. B. Calcutt (1995), The thermal structure and dynamics of the atmosphere of Venus between 70 and 90 km from the Galileo-NIMS spectra, *Icarus*, *114*, 300–309, doi:10.1006/icar.1995.1063.

Rothman, L., et al. (2005), The Hitran 2004 molecular spectroscopic database, *J. Quant. Spectrosc. Radiat. Transfer*, *96*, 139–204.

Siebenmorgen, R., et al. (2007), Very large telescope paranal science operations CRIRES user manual, *Rep. VLT-MAN-ESO-14500-3486*, 56 pp., Eur. South. Obs., Garching, Germany.

Stepanova, G. I., and G. M. Shved (1985), Radiation transfer in the 4.3-μm CO_2 band and the 4.7-μm CO band in the atmospheres of Venus and Mars with violation of LTE: Populations of vibrational states, *Sov. Astron., Engl. Transl.*, *29*, 248–422.

Svedhem, H., et al. (2007), Venus Express: The first European mission to Venus, *Planet. Space Sci.*, *55*, 1636–1652, doi:10.1016/j.pss.2007.01.013.

Taylor, F. W., et al. (1980), Structure and meteorology of the middle atmosphere of Venus infrared remote sensing from the Pioneer orbiter, *J. Geophys. Res.*, *85*, 7963–8006.

Titov, D. V., et al. (2006), Venus Express science planning, *Planet. Space Sci.*, *54*, 1279–1297, doi:10.1016/j.pss.2006.04.017.

A. Cardesín Moinelo and G. Piccioni, IASF, INAF, via del Fosso del Cavaliere 100, I-00133 Rome, Italy.

P. Drossart and S. Erard, Observatoire de Paris, F-92195 Meudon, France.

G. Gilli and M. A. López-Valverde, Instituto de Astrofísica de Andalucía, CSIC, Camino Bajo de Huetor 50, E-18008 Granada, Spain. (gilli@iaa.es)